Relativistic calculations for the exclusive photoproduction of η mesons from complex nuclei

M. Hedayati-Poor and H. S. Sherif

Department of Physics, University of Alberta, Edmonton, Alberta, Canada T6G 2J1

A relativistic model for the quasifree photoproduction of η mesons from complex nuclei is developed. The interactions between fields are introduced through effective Lagrangians. Contributions from several nucleon resonances as well as nucleon Born terms and vector meson exchange diagrams are included. Nucleon and η wave functions are solutions of Dirac and Klein-Gordon equations, respectively. Final state interactions of the outgoing particles are included via optical potentials. The effects of these interactions on the cross sections and photon asymmetries are studied and are found to be large. Calculations indicate that at energies near threshold the exclusive reaction takes place mainly through formation of the $S_{11}(1535)$ resonance. Comparisons with the nonrelativistic calculations show differences between the two approaches both for the cross sections and photon asymmetries. We give some detailed predictions for the reaction observables for exclusive photoproduction on ^{12}C, ^{16}O, and ^{40}Ca. [S0556-2813(97)05209-6]

I. INTRODUCTION

η meson production reactions explore a rich domain of phenomena at the interface of nuclear and particle physics. These reactions have the potential for expanding our understanding of the formation of nucleon resonances and their propagation in the nuclear medium. Moreover, as has been shown recently, these reactions have allowed more precise determination of the mass of the η meson and the study of its rare decays [1,2]. The spin-isospin characteristics of the η lead to a selectivity of resonance channels that can be formed through its interactions with a nucleon. At energies near the threshold of its production, there is a significant preference for the excitation of the $S_{11}(1535)$ resonance which is known to decay nearly 50% of the time to an η meson and a nucleon. By contrast, the $S_{11}(1650)$, which has identical characteristics, has only a decay rate below 2%. The understanding of these dissimilar branching ratios is still an open question and may be a reflection of important and subtle differences in the detailed substructures of these resonances. The selectivity mentioned above makes the η meson production reactions an important tool for studying the physics of the $S_{11}(1535)$ resonance.

Until recently the production of η mesons using photon beams has been largely confined to proton targets. The advent of high-duty-cycle electron accelerators such as those at the Jefferson Lab, Mainz, Bates and other laboratories, has opened up novel possibilities of performing production experiments on complex nuclei [3].

The elementary reaction $\gamma + p \rightarrow \eta + p$ has been the subject of several studies. Benmerrouche *et al.* [4] developed an effective Lagrangian approach to study this reaction. Contributions from nucleon resonances and *t*-channel vector mesons as well as the nucleon Born diagrams are included. Calculations were performed at the tree level and included eight free parameters. The $S_{11}(1535)$ was found to be the dominant contributor to the reaction at energies close to threshold. In addition, from comparisons with the data, the authors concluded that there is no clear preference for using pseudoscalar (PS) or pseudovector (PV) coupling forms for the interaction vertices of the η meson with the nucleon and nucleon resonances. Bennhold and Tanabe [5,6] developed a somewhat different approach to η photoproduction on the nucleon. They used a coupled channel isobar model, in which the reaction is related to (γ, π), (π, η), and (η, η) reactions. They included contributions from three resonances $S_{11}(1535)$, $P_{11}(1440)$, and $D_{13}(1520)$. The data on the elementary reaction appeared to favor the PS form of the ηNN vertex. The authors employed the resulting elementary amplitude to study coherent and incoherent photoproduction of η mesons on nuclei. This model for the elementary process was later extended by Tiator *et al.* [7] to include Born as well as ρ and ω exchange diagrams through effective Lagrangians. The resulting elementary amplitudes were subsequently used to calculate the PWIA (plane wave impulse approximation) amplitude of the photoproduction reaction on light nuclei.

The elementary amplitude mentioned above was also used by Lee *et al.* [8] to calculate the amplitude for quasifree photoproduction of η mesons on heavier nuclei. They performed exclusive as well as inclusive reaction calculations using a nonrelativistic approach. The initial bound nucleon is described by a harmonic oscillator wave function and final state interactions of the outgoing particles with the recoil nucleus are introduced through optical potentials. Two different optical potentials were used for the η mesons. The authors found that the photon asymmetry is insensitive to the final state interactions of the outgoing particles as well as the size of the target nucleus.

In this paper we develop a relativistic model for the $(\gamma, \eta p)$ reaction on nuclei leading to specific final states of the residual nuclei (exclusive reactions). The study of the photoproduction reactions on nuclei compliments the ongoing studies of the production on free nucleons. In addition to further investigating the reaction mechanism, studies on nuclei can help limit any existing ambiguities in the elementary process. Moreover, since the production process is mediated by certain nucleon resonances and vector mesons, these studies open the possibility of investigating medium modifications of the properties of these hadrons in nuclei. As men-

tioned earlier, the availability of a new generation of accelerators capable of producing high quality beams of electrons and photons has led to increased interest in eta photoproduction physics. Many experiments that were not possible in the past are now within reach.

The present work is devoted to quasifree photoproduction. This type of reaction has the advantage of allowing measurements at small momentum transfer to the residual nucleus. This, in addition to enhancing the possibility of increased cross sections, compliments the information obtained from coherent and incoherent (γ, η) reactions which by necessity involve large momentum transfers.

In the present study we follow a relativistic approach. This is motivated by the impressive successes of the relativistic mean field approach to nuclear dynamics. We have recently studied the difference between relativistic and nonrelativistic treatments in photonuclear knockout [9] and quasielastic scattering of electrons [10], and have found that there are important differences between the two approaches. In the course of the present study we shall compare our results to those of the work of Lee *et al.* [8].

The main ingredients of the present treatment are as follows. The effective Lagrangian of Benmerrouche *et al.* [4] is used for the interactions between fields. Contributions from nucleon resonances and t-channel vector mesons as well as the nucleon Born diagrams are included. In addition to the $S_{11}(1535)$ resonance, we also include three spin-$\frac{1}{2}$ resonances $[P_{11}(1440), S_{11}(1650), P_{11}(1710)]$ and one spin-$\frac{3}{2}$ resonance $[D_{13}(1520)]$. The nuclear wavefunctions are solutions of the Dirac equation with strong scalar and vector potentials in the spirit of the relativistic mean field theory of Walecka [11,12]. Calculations are carried out in the PWIA limit and also in the distorted wave approximation (DWA) in which the final state interactions are taken into account. Bennhold and Wright have developed a similar model for the photoproduction of kaons on nuclei [13]. A short note on the present work was reported earlier [14].

In the following section we derive the amplitude of the $A(\gamma, \eta p)A-1$ reaction and calculate the relevant observables. The results of our calculations are presented in Sec. III and our conclusions are given in Sec. IV.

II. FORMALISM

The model for the $(\gamma, \eta p)$ reaction on nuclei has the incident photon interacting with a bound proton through some process denoted by the blob in Fig. 1. A proton and an η meson are produced. The diagrams contributing to the blob of Fig. 1, at the tree level, are shown in Fig. 2. The Born diagrams (s and u channels of the nucleon propagator) are shown in Figs. 2(a) and 2(b), the t-channel vector meson diagram is shown in Fig. 2(c), and Figs. 2(d) and 2(e) are the nucleon resonance poles.

The starting point in the present approach is a relativistic interaction Lagrangian for a system of photons, nucleons, and mesons from which one obtains the transition amplitude for the $A(\gamma, \eta p)A-1$ reaction. The amplitude then is used to calculate the observables for the reaction.

A. Interaction Lagrangian

In the photoproduction of η mesons from complex nuclei, the reaction is taking place within the nuclear medium. The
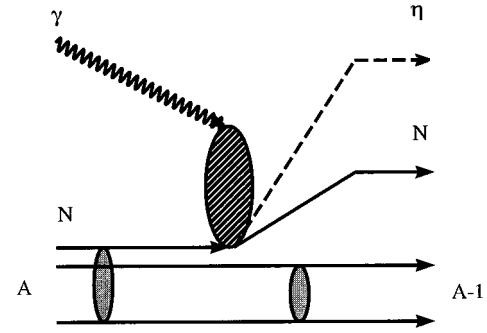

FIG. 1. Feynman diagram for an $A(\gamma, \eta p)A-1$ reaction. The incident photon with momentum **k** is absorbed by a proton embedded in nucleus A, resulting in ejection of a proton and an η meson.

dynamics of the nucleons within the nuclear matter is described through the relativistic mean field Lagrangian of Walecka [11,12]. The η meson is described by solutions to the Klein-Gordon equation. The interactions of the fields involved in the production reaction depicted in Fig. 2, are described through the interaction Lagrangian

$$\mathcal{L}_{\text{int}} = \mathcal{L}_{\eta NN} + \mathcal{L}_{\gamma NN} + \mathcal{L}_{V\eta\gamma} + \mathcal{L}_{VNN} + \mathcal{L}_{\eta NR} + \mathcal{L}_{\gamma NR}. \tag{2.1}$$

In the present work we adopt the pseudoscalar form for the η meson-nucleon states coupling. This choice is based on the work of Bennhold and Tanabe [6] and Lee *et al.* [8] which showed preference for this form in the production on pro-
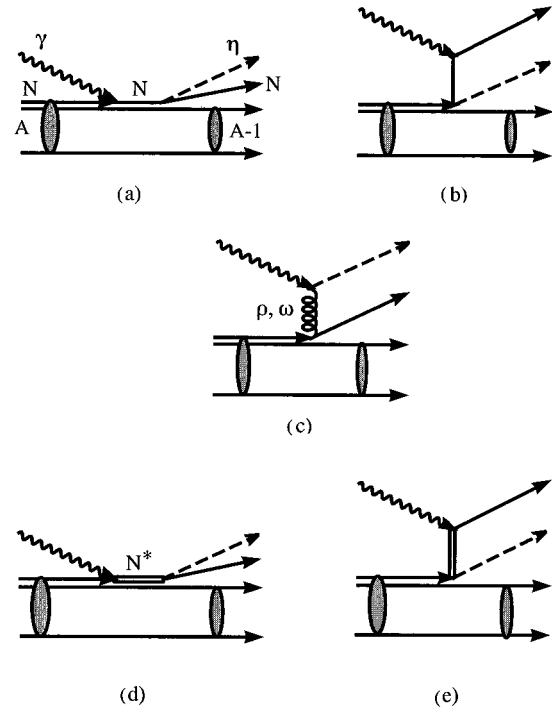

FIG. 2. The contributing Feynman diagrams to $A(\gamma, \eta p)A-1$ reaction. (a) and (b) are the s- and u-channel Born diagram respectively, (c) the t-channel vector meson diagram, and (d) and (e) are the s- and u-channel nucleon resonance poles.

tons. The interaction Lagrangians which involve the nucleon and spin-$\frac{1}{2}$ resonances are cast in the following forms [4]:

$$\mathcal{L}_{\eta NN} = -ig_{\eta}\bar{\psi}\gamma_5\psi\eta, \qquad (2.2)$$

$$\mathcal{L}_{\gamma NN} = -e\bar{\psi}\gamma_{\mu}A^{\mu}\psi - \frac{e\kappa_p}{4M}\bar{\psi}\sigma^{\mu\nu}\psi F_{\mu\nu}, \qquad (2.3)$$

$$\mathcal{L}_{VNN} = -g_v\bar{\psi}\gamma_{\mu}\psi V^{\mu} - \frac{g_t}{4M}\bar{\psi}\sigma_{\mu\nu}\psi V^{\mu\nu}, \qquad (2.4)$$

$$\mathcal{L}_{V\eta\gamma} = \frac{e\lambda_V}{4m_{\eta}}\epsilon_{\mu\nu\lambda\sigma}F^{\mu\nu}V^{\lambda\sigma}\eta, \qquad (2.5)$$

$$\mathcal{L}_{\eta NR} = -ig_{\eta NR}\bar{\psi}\Gamma R\eta + \text{H.c.}, \qquad (2.6)$$

$$\mathcal{L}_{\gamma NR} = -\frac{e\kappa_p^R}{2(M_R+M)}\bar{R}\Gamma^{\mu\nu}\psi F_{\mu\nu} + \text{H.c.}, \qquad (2.7)$$

where

for S_{11} resonances $\Gamma = 1$ and $\Gamma^{\mu\nu} = \gamma_5\sigma^{\mu\nu}$,

for P_{11} resonances $\Gamma = \gamma_5$ and $\Gamma^{\mu\nu} = \sigma^{\mu\nu}$, $\qquad (2.8)$

κ_p and κ_p^R are the anomalous magnetic moment of the proton and the nucleon (proton) resonance, respectively, and M_R is the resonance mass. The tensor $V_{\mu\nu}(x)$ is related to the vector meson field V_{μ} by

$$V_{\mu\nu}(x) = \partial_{\mu}V_{\nu}(x) - \partial_{\nu}V_{\mu}(x). \qquad (2.9)$$

The interactions of photons and η mesons with the spin-$\frac{3}{2}$ $[D_{13}(1520)]$ resonance are introduced through the Lagrangians

$$\mathcal{L}_{\eta NR} = \frac{f_{\eta NR}}{m_{\eta}}\bar{R}^{\mu}\theta_{\mu\nu}(Z)\gamma_5\psi\partial^{\nu}\eta + \text{H.c.}, \qquad (2.10)$$

$$\mathcal{L}_{\gamma NR}^1 = \frac{ie\kappa_R^1}{2M}\bar{R}^{\mu}\theta_{\mu\nu}(Y)\gamma_{\lambda}\psi F^{\nu\lambda} + \text{H.c.}, \qquad (2.11)$$

$$\mathcal{L}_{\gamma NR}^2 = \frac{e\kappa_R^2}{4M^2}\bar{R}^{\mu}\theta_{\mu\nu}(X)\partial_{\lambda}N F^{\nu\lambda} + \text{H.c.}, \qquad (2.12)$$

where R^{μ} is the field associated with the $D_{13}(1520)$ resonance. Two anomalous magnetic moments κ_R^1 and κ_R^2 are used in conjunction with the two different interaction Lagrangians introduced by Benmerrouche *et al.* [4] for the $\gamma\eta R$ vertex. The function $\theta_{\mu\nu}(V)$ is given by

$$\theta_{\mu\nu}(V) = g_{\mu\nu} + \left[-\frac{1}{2}(1+4V)+V\right]\gamma_{\mu}\gamma_{\nu},$$

$$V = X, Y, Z, \qquad (2.13)$$

TABLE I. Summary of the properties of the baryon resonances included in present model. J^{π} is the spin parity, and L is the relative angular momentum related to πN scattering state. The subscripts I and J for the L values (third column) represent the isospin and total angular momentum assigned to the resonance, respectively. Γ is the total width of the resonance.

Resonance	J^{π}	L_{2I2J}	Mass (MeV)	Γ (MeV)
$N^*(1440)$	$1/2^+$	P_{11}	1440	350
$N^*(1520)$	$3/2^-$	D_{13}	1520	120
$N^*(1535)$	$1/2^-$	S_{11}	1535	150
$N^*(1650)$	$1/2^-$	S_{11}	1650	150
$N^*(1710)$	$1/2^+$	P_{11}	1710	100

where the parameters X, Y, and Z, often referred to as off-shell parameters, are obtained by fitting the experimental data for the elementary reaction.

The authors of Ref. [4], through fits to existing data, provided several sets of values for the parameters and observables related to the coupling constants of the effective interaction Lagrangians of Eqs. (2.2)–(2.12). The parameters we use are those of the second column of Table V of the above reference. These parameters are associated with the PS coupling which is the form used in the present work. The off-shell parameters α, β, and δ given in that table are related to the X, Y, and Z introduced in Eqs. (2.10)–(2.12), as

$$\alpha = 1+4Z, \quad \beta = 1+4y, \quad \delta = 1+2X. \qquad (2.14)$$

A total of five nuclear resonances are included in the present calculations. Table I gives some of the properties of these resonances.

B. Reaction amplitude

At the tree level the S matrix for the $A(\gamma,\eta p)A-1$ reaction is [15]

$$S_{fi} = -\frac{1}{2}\int \langle f|T[\mathcal{L}_{\text{int}}(x)\mathcal{L}_{\text{int}}(y)]|i\rangle d^4x d^4y, \qquad (2.15)$$

where $|i\rangle$ and $|f\rangle$ are the initial and final states of the system, respectively. The T in front of the square brackets denotes the time-ordered product of the operators within the brackets. We shall illustrate, below, the derivation of the S matrix for one of the contributing diagrams of Fig. 2, namely, the S_{11} diagram. The same procedure can be used to derive the S matrix for the other diagrams.

After introducing $\mathcal{L}_{\gamma NR}$ and $\mathcal{L}_{\eta NR}$ [from Eqs. (2.6), (2.7), and (2.8)] and using Wick's theorem [15], the S matrix for the S_{11} resonance diagrams can be written as

$$S_{fi}^R = -\frac{ie\kappa_p^R g_{\eta NR}}{2(M+M_R)}\int \langle f|N[\bar{\psi}(y)\eta(y)\underline{R(y)\bar{R}(x)}$$

$$\times \gamma_5\sigma_{\mu\nu}F^{\mu\nu}(x)\psi(x)$$

$$+ \bar{\psi}(x)\gamma_5\sigma_{\mu\nu}F^{\mu\nu}(x)\underline{R(x)\bar{R}(y)}\psi(y)\eta(y)]|i\rangle dx^4 dy^4.$$

$$(2.16)$$

The initial state $|i\rangle$ contains a photon and a target nucleus with A nucleons. The latter is regarded as made up of a core and a valance nucleon. We write

$$|i\rangle = a_{s_\gamma}^\dagger(\mathbf{k}_\gamma) \sum_{J_B M_B J} (J, J_B; M, M_B | J_i, M_i)$$

$$\times [\mathcal{S}_{J_i J_f}(J_B)]^{1/2} b_{J_B M_B}^\dagger | \phi_J^M \rangle, \qquad (2.17)$$

where $a_{s_\gamma}^\dagger(\mathbf{k}_\gamma)$ is the creation operator for a photon with momentum $\mathbf{k}_\gamma$ and polarization s_γ. $b_{J_B M_B}^\dagger$ creates a nucleon with angular momentum quantum numbers J_B and M_B bound to the core $|\phi_J^M\rangle$ and $\mathcal{S}$ is the corresponding spectroscopic factor.

The final state $|f\rangle$, composed of an η meson, a nucleon, and the residual nucleus, is written in a similar fashion using creation operators for the η and the nucleon. To reduce the complexity of the numerical calculations we use the plane wave approximation for the propagators [16]. In this approximation the propagator for a spin-$\frac{1}{2}$ resonance assumes the simple form

$$\underline{R(x)\bar{R}(y)} = iS_R^F(x-y) = i\frac{\not{k}_R + M_R}{k_R^2 - M_R^2}\delta^4(x-y), \qquad (2.18)$$

where $S_R^F(x-y)$ is the Feynman propagator of a nucleon resonance with mass M_R and four-momentum k_R. Carrying out the Fock space calculations and using the radiation gauge, the S matrix of Eq. (2.16) reduces to the form

$$S_{fi}^R = \frac{e}{(2\pi)^{9/2}}\left(\frac{M}{E_p}\frac{1}{2E_\eta}\frac{1}{2E_\gamma}\right)^{1/2} \sum_{J_B M_B} (J_f, J_B; M_f, M_B | J_i, M_i)$$

$$\times [\mathcal{S}_{J_i J_f}(J_B)]^{1/2} \int d^4x \Psi_{s_f}^{(-)\dagger}(x) \Gamma_{S_{11}}$$

$$\times \Psi_{J_B M_B}(x) \varphi_\eta^*(x) e^{-ik_\gamma \cdot x}, \qquad (2.19)$$

where $\Gamma_{S_{11}}$ is a 4×4 matrix operator and contains combinations of the Dirac γ matrices, polarization of the interacting photon, mass, and four-momentum of the propagating resonance. The explicit form of this operator for each of the contributing diagrams is given below. In the above equation, E_γ, E_p, and E_η are energies of the photon, proton, and η meson, respectively, and M is proton mass. $\Psi_{J_B, M_B}(x)$ describes a bound nucleon and is a solution of Dirac equation with the appropriate strong scalar and vector potentials. $\Psi_{s_f}(x)$ is the wave function of the outgoing proton which in the plane wave approximation is just a plane wave Dirac spinor. In the distorted wave calculations $\Psi_{s_f}(x)$ is a solution of the Dirac equation with the strong vector and scalar optical potentials. The η meson wave function φ_η is a solution of the Klein-Gordon equation with an appropriate optical potential for the η-nucleus system.

The structure of the total S matrix is the same as S_{fi}^R of Eq. (2.19) except for $\Gamma_{S_{11}}$ which must be replaced by a sum representing contributions from all the diagrams included in the model (Fig. 2). We obtain the following operators for these diagrams:

$$\Gamma_{\text{proton}} = g_{\eta NN}\gamma_0\left(\gamma_5\frac{\not{k}_s + M}{k_s^2 - M^2}\left(\frac{\kappa_p}{2M}\not{k}_\gamma + 1\right)\not{\epsilon}_r + \left(\frac{\kappa_p}{2M}\not{k}_\gamma + 1\right)\not{\epsilon}_r\frac{\not{k}_u + M}{k_u^2 - M^2}\gamma_5\right), \qquad (2.20)$$

$$\Gamma_{S_{11}} = \frac{g_{\eta NR}\kappa_p^R}{M + M_R}\gamma_0\left(\frac{\not{k}_s + M_R}{k_s^2 - M_R^2}\gamma_5\not{k}_\gamma\not{\epsilon}_r + \gamma_5\not{k}_\gamma\not{\epsilon}_r\frac{\not{k}_u + M_R}{k_u^2 - M_R^2}\right), \qquad (2.21)$$

$$\Gamma_{P_{11}} = \frac{g_{\eta NR}\kappa_p^R}{M + M_R}\gamma_0\left(\gamma_5\frac{\not{k}_s + M_R}{k_s^2 - M_R^2}\not{k}_\gamma\not{\epsilon}_r + \not{k}_\gamma\not{\epsilon}_r\frac{\not{k}_u + M_R}{k_u^2 - M_R^2}\gamma_5\right), \qquad (2.22)$$

$$\Gamma_V^v = -i\frac{\lambda_v g_v}{m_\eta}\epsilon_{\mu\nu\lambda\sigma}\gamma_0\frac{\epsilon^\mu k_\gamma^\nu k_\eta^\lambda \gamma^\sigma}{k_t^2 - m_V^2}, \qquad (2.23)$$

$$\Gamma_V^t = \frac{\lambda_t g_t}{2Mm_\eta}\epsilon_{\mu\nu\lambda\sigma}\gamma_0\frac{\epsilon^\mu k_\gamma^\nu \sigma^{\sigma\alpha}k_{t\alpha}k_\eta^\lambda}{k_t^2 - m_V^2}, \qquad (2.24)$$

$$\Gamma_{D_{13}}^{(1)} = -\frac{f_{\eta NR}\kappa_R^{(1)}}{2Mm_\eta}\gamma_0\left(\gamma_5 k_\eta^\nu \theta_{\nu\mu}(Z)\frac{\not{k}_s + M_R}{k_s^2 - M_R^2}P^{\mu\alpha}\theta_{\alpha\beta}(Y)\gamma_\lambda(k_\gamma^\beta\epsilon_r^\lambda - \epsilon_r^\beta k_\gamma^\lambda) + \gamma_\lambda\theta_{\beta\alpha}(Y)(k_\gamma^\beta\epsilon_r^\lambda - \epsilon_r^\beta k_\gamma^\lambda)\right.$$

$$\left.\times\frac{\not{k}_u + M_R}{k_u^2 - M_R^2}P^{\alpha\mu}\theta_{\mu\nu}(Z)k_\eta^\nu\gamma_5\right), \qquad (2.25)$$

$$\Gamma^{(2)}_{D_{13}} = \frac{f_{\eta NR}\kappa^{(2)}_R}{4m_\eta M^2}\,\gamma_0\Bigg(\gamma_5 k^\nu_\eta \theta_{\nu\mu}(Z)\frac{k_s+M_R}{k^2_s-M^2_R}P^{\mu\alpha}\theta_{\alpha\beta}(X)(k^\beta_\gamma\epsilon^\lambda_r - \epsilon^\beta_r k^\lambda_\gamma)\{k^B\}_\lambda + \{k_p\}_\lambda\theta_{\beta\alpha}(X)(k^\beta_\gamma\epsilon^\lambda_r - \epsilon^\beta_r k^\lambda_\gamma)$$

$$\times\frac{k_u+M_R}{k^2_u-M^2_R}P^{\alpha\mu}\theta_{\mu\nu}(Z)k^\nu_\eta\gamma_5\Bigg), \tag{2.26}$$

where

$$P^{\mu\nu} = \Bigg(g^{\mu\nu} - \frac{1}{3}\gamma^\mu\gamma^\nu - \frac{1}{2M_R}[\gamma^\mu k^\nu - \gamma^\nu k^\mu] - \frac{2}{3M^2_R}k^\mu k^\nu\Bigg), \tag{2.27}$$

and k^B is the local momentum of the bound nucleon, and

$$k_s = k_\eta + k_p,\quad k_t = k_\gamma - k_\eta,\quad k_u = k_p - k_\gamma. \tag{2.28}$$

1. Plane wave calculations

To calculate the amplitude of Eq. (2.19) one can use either plane waves or distorted waves to describe the outgoing particles. In the plane wave approximation the final state interactions of the outgoing nucleon and η meson, with the recoil nucleus, are ignored. The respective wave functions have the form

$$\psi_p(k_p,x) = \sqrt{\frac{E+M}{2M}}\begin{pmatrix}1\\[2pt]\dfrac{\boldsymbol{\sigma}\cdot\boldsymbol{k}_p}{E+M}\end{pmatrix}e^{-ik_p\cdot x}\chi_{s_f},$$

$$\varphi_\eta(x) = e^{-ik_\eta\cdot x}. \tag{2.29}$$

Thus in the plane wave approximation (PWA) the S matrix in Eq. (2.19) takes the form

$$S^R_{fi} = \frac{e}{(2\pi)^{7/2}}\Bigg(\frac{M}{E_p}\frac{1}{2E_\eta}\frac{1}{2E_\gamma}\Bigg)^{1/2}\delta(E_B+E_\gamma-E_p-E_\eta)\sum_{J_B M_B}(J_f,J_B;M_f,M_B|J_i,M_i)$$

$$\times[\mathcal{S}_{J_i J_f}(J_B)]^{1/2}\int d^3x\, u^\dagger_{s_f}(k_p)e^{ik_{\text{rec}}\cdot x}\Gamma_{S_{11}}\Psi_{J_B M_B}(x), \tag{2.30}$$

where k_{rec} is the momentum of the recoil nucleus ($k_{\text{rec}} = k_\gamma - k_p - k_\eta$). Equation (2.30) shows that the PWA S matrix is made up of terms proportional to the Fourier transform of the components of the bound state wave function.

2. Final state interactions: Distorted wave calculations

The rest of this section is devoted to a derivation of the form of the S matrix in the distorted wave approximation (DWA). The continuum nucleon wave function is written as

$$\psi^{(-)\dagger}_{s_f}(x) = 4\pi\Bigg[\frac{E+M}{2M}\Bigg]^{1/2}e^{iEt}\sum_{LJM}i^{-L}Y^{M-s_f}_L(\hat{\mathbf{k}}_f)\mathcal{Y}^{M\dagger}_{L1/2J}(\Omega)(L,1/2;M-s_f,s_f|J,M)\Big[f_{LJ}(r),\quad i\sigma\cdot\hat{\mathbf{r}}g_{LJ}(r)\Big], \tag{2.31}$$

where f_{LJ} and g_{LJ} refer to the upper and lower radial functions. These are solutions of the radial Dirac equation with vector and scalar optical potentials obtained from comparison with proton-nucleus elastic scattering data. More details of the Dirac proton wavefunctions can be found in Ref. [16]. Expanding the eta and photon wave functions into partial waves and using these in the expression of the amplitude given by Eq. (2.19), one gets the DWA S matrix as

$$S_{fi} = \frac{e}{\pi}\Bigg(\frac{E_p+M}{E_p E_\eta E_\gamma}\Bigg)^{1/2}\delta(E_B+E_\gamma-E_p-E_\eta)\sum_{J_B M_B}(J_f,J_B;M_f,M_B|J_i,M_i)[\mathcal{S}_{J_i J_f}(J_B)]^{1/2}\sum_{LJL_\eta L_\gamma}i^{L_\gamma-L-L_\eta}(2L_\gamma+1)^{1/2}$$

$$\times\sum_{MM_\eta}Y^{M-s_f}_L(\hat{\mathbf{k}}_p)[Y^{M_\eta}_{L_\eta}(\hat{\mathbf{k}}_\eta)]^*\Bigg(L,\frac{1}{2};M-s_f,s_f\Big|J,M\Bigg)$$

$$\times \times \left\{ R_{ff}[\kappa \kappa_B L_\eta L_\gamma] A_{11} \begin{bmatrix} \kappa & \kappa_B & L_\eta \\ M & M_B & M_\eta \end{bmatrix} L_\gamma \; \xi \right] + i R_{fg}[\kappa \kappa_B L_\eta L_\gamma] A_{12} \begin{bmatrix} \kappa & \kappa'_B & L_\eta \\ M & M_B & M_\eta \end{bmatrix} L_\gamma \; \xi \right]$$

$$- i R_{gf}[\kappa \kappa_B L_\eta L_\gamma] A_{21} \begin{bmatrix} \kappa' & \kappa_B & L_\eta \\ M & M_B & M_\eta \end{bmatrix} L_\gamma \; \xi \right] + R_{gg}[\kappa \kappa_B L_\eta L_\gamma] A_{22} \begin{bmatrix} \kappa' & \kappa'_B & L_\eta \\ M & M_B & M_\eta \end{bmatrix} L_\gamma \; \xi \right] \right\}, \qquad (2.32)$$

where $\kappa = (L-J)(2J+1)$ and $L' = 2J - L$. The radial integrals are given by

$$R_{CB}[\kappa \kappa_B L_\eta L_\gamma]$$

$$= \int C_{LJ}(r) B_{L_B M_B}(r) v_{L_\eta}(k_\eta r) j_{L_\gamma}(k_\gamma r) r^2 dr, \qquad (2.33)$$

and $C(r)$ is either an upper- or lower-component radial function for the ejected proton while $B(r)$ is the counterpart for the bound state wave function. The angular integrals are given as follows:

$$A_{ij} \begin{bmatrix} \kappa' & \kappa_B & L_\eta \\ M & M_B & M_\eta \end{bmatrix} L_\gamma \; \xi \right]$$

$$= \int (\mathcal{Y}^M_{L1/2J})^\dagger \Gamma_{ij} \mathcal{Y}^{M_B}_{L_B 1/2J_B} Y^{M_\eta}_{L_\eta}(\Omega) Y^0_{L_\gamma}(\Omega) d\Omega. \quad (2.34)$$

The matrix operators Γ_{ij} are the elements of the 4×4 Γ matrix operator

$$\Gamma = \begin{pmatrix} \Gamma_{11} & \Gamma_{12} \\ \Gamma_{21} & \Gamma_{22} \end{pmatrix}. \qquad (2.35)$$

C. Observables

It is useful to define a function of the initial and final spin projections $Z^{s_f}_{\xi M_B}$ by rewriting the amplitude of Eq. (2.32) in the form

$$S_{fi} = \frac{e}{\pi} \left(\frac{E_p + M}{E_p E_\eta E_\gamma} \right)^{1/2} \delta(E_p + E_\gamma - E_B - E_\eta)$$

$$\times \sum_{J_B M_B} (J_f, J_B; M_f, M_B | J_i, M_i) [\mathcal{S}_{J_i J_f}(J_B)]^{1/2} Z^{s_f}_{\xi M_B}. \qquad (2.36)$$

The triple differential cross section is related to $Z^{s_f}_{\xi M_B}$ by

$$\frac{d^3\sigma}{d\Omega_\eta d\Omega_p dE_\eta}$$

$$= \frac{8 \alpha \pi}{\hbar c} \left[\frac{E_p + M c^2}{E_\gamma} \right] k_p c k_\eta c \frac{1}{R} \sum_{J_B M_B s_f \xi} \frac{\mathcal{S}_{J_i J_f}(J_B)}{2J_B + 1} |Z^{s_f}_{\xi M_B}|^2, \qquad (2.37)$$

where α is the fine structure constant and the recoil factor R is defined in a manner similar to the case of $(e,e'p)$ reactions [17],

$$R = 1 - \frac{E_p}{E_r} \frac{1}{|\mathbf{k}_p|^2} \mathbf{k}_p \cdot \mathbf{k}_r, \qquad (2.38)$$

and E_r is the total energy of the residual nucleus.

The photon asymmetry for linearly polarized incident photons is

$$A = \frac{d\sigma_\parallel - d\sigma_\perp}{d\sigma_\parallel + d\sigma_\perp}, \qquad (2.39)$$

where $d\sigma_\parallel$ and $d\sigma_\perp$ are the cross section for specified polarizations of the incident photon, namely, parallel and perpendicular to the plane of the reaction.

III. RESULTS AND DISCUSSION

This paper is concerned with the study of the exclusive quasifree $(\gamma, \eta p)$ reaction on complex nuclei. To date there are no available experimental data for this particular reaction (data exist only for inclusive reactions [3]). Since the lack of attempts to measure the exclusive observables is mainly due to the expectation of low cross sections, it is of practical importance to identify the kinematical regions in which the cross sections are relatively large. Figure 3 shows the calculated cross section for this reaction on ^{12}C leading to the ground state of ^{11}B (assumed to be a pure $p_{3/2}$ hole state). The incident photon energy is 750 MeV. The calculations are carried out in the plane wave approximation for the outgoing
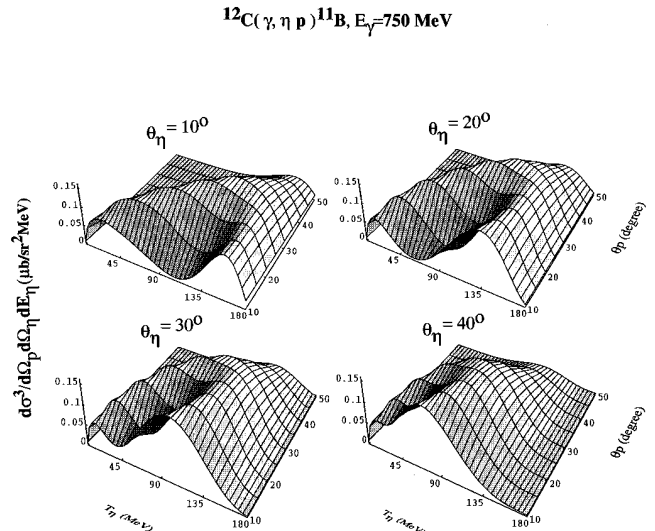
^{12}C($\gamma, \eta p$)^{11}B, E_γ=750 MeV

FIG. 3. The cross section for the ^{12}C($\gamma, \eta p$)^{11}B$_{g.s.}$ reaction for the regions of the phase space where the reaction has significant yield. Calculations are performed in the plane wave approximation.

proton and η meson. The bound nucleon is described by a solution of the Dirac equation involving the relativistic scalar and vector Hartree potentials of Ref. [18]. We used the maximum possible value for the spectroscopic factor (i.e., $2J_B +1$; J_B is the total angular momentum of the bound proton). The azimuthal angles of the outgoing proton and η meson are fixed at 180° and 0°, respectively. Calculations are performed at four different polar angles for the η meson and cover the outgoing proton polar angular range 10°–50°. Cross sections are plotted as a function of polar angle of the outgoing proton and the kinetic energy of the η meson. These results indicate that one can observe relatively large cross sections for θ_η in the range 10°–30° and $\theta_p = 15°–30°$. The pair of angles $\theta_\eta = \theta_p = 30°$ may be a preferable setting experimentally and hence will be used for most of the analysis done here. Similar results were found for ^{16}O and ^{40}Ca nuclei. These results are expected to change somewhat with respect to variation in the incident photon energy. The larger cross sections will shift towards more forward angles as the photon energy increases.

It is well known that the eta photoproduction reaction on the proton near threshold is dominated by the $S_{11}(1535)$ resonance formation. We have done calculations aimed at assessing the extent to which this dominance prevails when the reaction takes place within the nuclear medium. The calculations are done for the reaction discussed above, again in the plane wave limit, where the angles of the outgoing particles are fixed at $\theta_\eta = \theta_p = 30°$. We varied the energy of the incident photon from near threshold to the energy where the contributions from the $S_{11}(1535)$ diagrams are comparable to contributions from all other diagrams. Results of these calculations are illustrated in Fig. 4: The dotted curves give the cross sections due to the formation of the $S_{11}(1535)$; contributions due to the rest of the diagrams are represented by solid curves. Note the varying scale for the cross section axes. Figure 4 shows that the $S_{11}(1535)$ resonance dominates the cross section from threshold up to a photon energy of about 1.1 GeV. The cross section is small at energies near threshold and increases with increasing photon energy, reaching its largest values in the photon energy range 750–950 MeV. At energies higher than 950 MeV, the cross section due to the $S_{11}(1535)$ resonance decreases as the photon energy increases.

In Fig. 5 we show the relative contributions of the individual diagrams. The cross section arising from the $S_{11}(1535)$ pole diagrams, shown by the long dashed curve, is clearly the dominant contribution. The second largest contribution comes form the proton poles (double-dash–double-dotted curve). The results of the calculations for the $D_{13}(1520)$ resonance and the vector mesons poles are shown by dot-dot-dashed and dot-dash-dashed curves, respectively. The solid curve shows the total cross section (i.e., contributions from all the diagrams). Besides confirming clearly that the $S_{11}(1535)$ resonance is the main contributor to the reaction in this energy region, these results also give us an indication of the relative importance of other diagrams. The next largest contribution comes from the proton pole followed by the D_{13} resonance, then the vector meson diagrams. The $P_{11}(1440)$, $S_{11}(1650)$, and $P_{11}(1710)$ resonances do not make significant contributions to the reaction at this energy.

In order to establish that the above conclusions are not affected by the inclusion of the final state interactions of the outgoing particles with the residual nucleus, we carried out distorted wave calculations in which these final state interactions are taken into account. Appropriate optical potentials are used in the calculation of the wave functions of the outgoing proton and η meson. In all the distorted wave calculations presented here the global optical potentials of Cooper et al. [19] have been used to calculate the Dirac distorted wave functions of the outgoing proton. For the outgoing η meson we use the Klein-Gordon equation together with the optical potentials of Refs. [8,22]. The results are shown in Fig. 6; the solid curve shows the cross section due to the $S_{11}(1535)$ resonance, whereas the dashed curve includes all contributions other than those of the $S_{11}(1535)$. These results indicate that, as in the plane wave calculations discussed above, the $S_{11}(1535)$ resonance is the dominant contributor to the reaction in the distorted wave limit. Note the general suppression of the cross section as a result of the inclusion of the final state interactions.

Figure 7 shows the calculated observables for the reaction where we investigate separately the effects of the proton and η meson final state interactions. The energy-dependent global optical potential of Cooper et al. [19] and the optical potential DW1 of Ref. [8] are used for outgoing protons and η mesons, respectively. Plane wave and various distorted wave calculations are shown. The comparisons of the cross sections are shown in Fig. 7(a) and those for the photon asymmetry are shown in Fig. 7(b). The short dashed curve shows the suppression due to the final state interaction of the outgoing proton with the residual nucleus. This suppression is more evident at higher η energies. These correspond to smaller energies of the outgoing protons and indicate that these protons are more affected by the distortion. This same qualitative behavior holds for the η meson distortion (dashed curve); the suppression is skewed towards smaller η energies. The dotted curve is the calculated cross section when distortion effects are included for both of the outgoing particles. The suppression of the cross section in this case is much more pronounced.

Figure 7(b) shows the photon asymmetry for the same reaction [see Eq. (2.39)]. Plane wave calculations (solid curve) produce a nearly flat curve for the photon asymmetry. Distortion of the outgoing η meson affects the shape and magnitude of the photon asymmetry only slightly. Inclusion of the final state interactions of the outgoing proton results in larger changes in the asymmetry. When both final state interactions are included, the resulting curve (dotted curve) has characteristics close to the case when only the proton is distorted.

Figure 8 shows the effects of different η optical potentials on the calculated observables. The curves of Fig. 8 are obtained with the same bound and continuum proton potentials while different optical potentials are used for the outgoing η meson. Five different potentials are used. The first two are those (denoted by DW1 and DW2) used by Lee et al. [8]. These are obtained in a $t\rho$ approximation using ηN t matrices obtained in a coupled channel approach [6,7,20] (a recent work by Batinić et al. [21] points out to a sign error in their analysis in [20] which may mean that the potential DW2 is not reliable). The other sets of potentials are those of Chiang et al. [22]. These are obtained by calculating the η self-
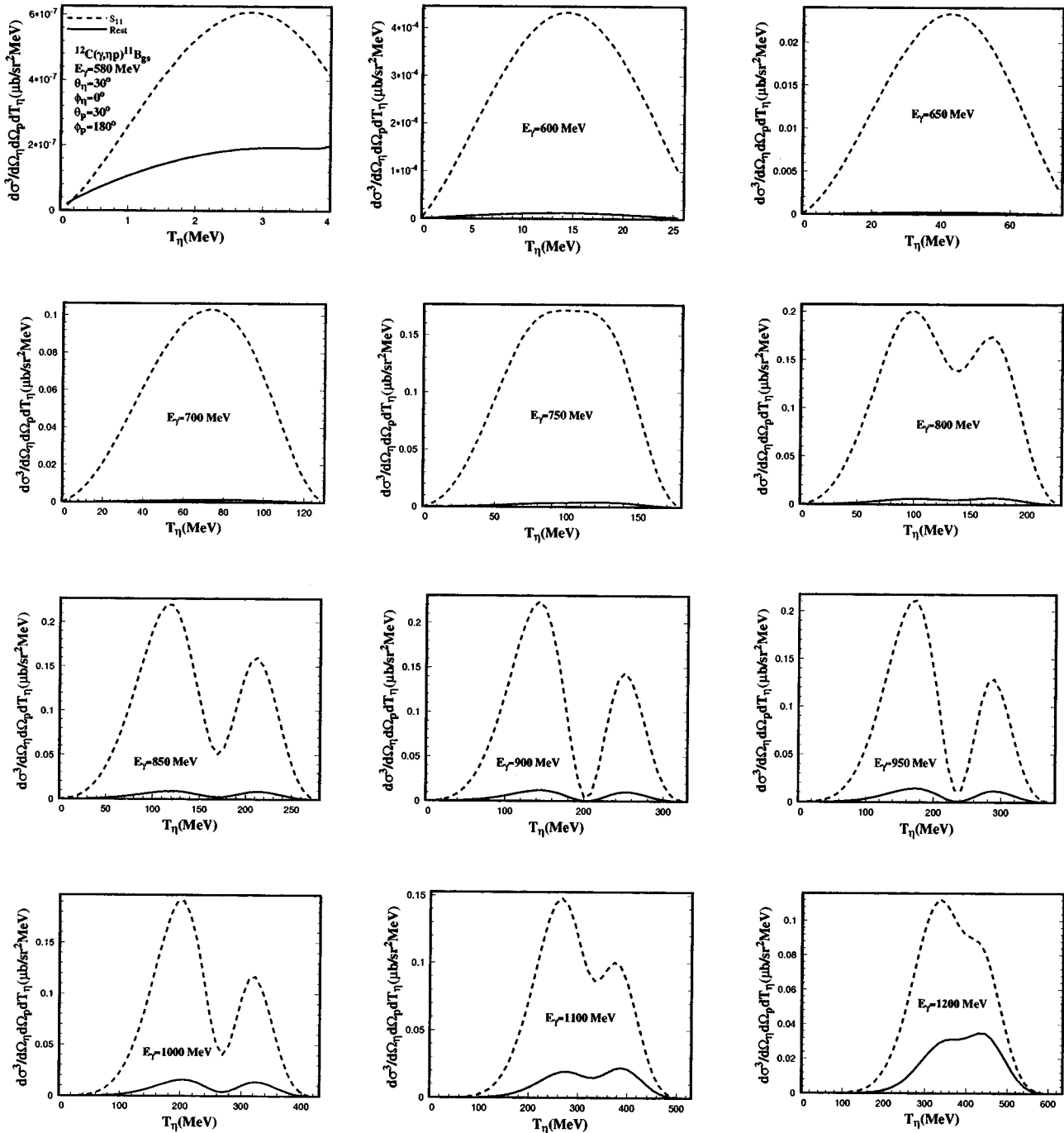
FIG. 4. The plane wave cross sections for the ^{12}C$(\gamma, \eta p)^{11}$B$_{g.s.}$ reaction for photon energies from near threshold up to 1.2 GeV.

energy in nuclear matter taking into account only contributions from the S_{11} resonance. The three different potentials used correspond to three different choices of the real part of the N^* self-energy [namely, Re$\Sigma_{N^*} = (\rho/\rho_0)V_{N^*}$ with $V_{N^*} = 50, 0, -50$ MeV; ρ and ρ_0 are the nuclear density for finite and infinite nuclear matter, respectively]. The uncertainty about the parameter V_{N^*} is a drawback for the potentials of Chiang *et al.*

In general the calculated cross sections show some dependence on the type of distorting potential used; there are some variations in shape and magnitude. The magnitude of the cross section obtained with the DW1 potential is somewhat

larger than those predicted by the other potentials near the midrange of η energies.

The corresponding calculations for photon asymmetry with different optical potentials for the outgoing η meson are shown in Fig. 8(b). All potentials produce approximately the same shape and magnitude for the photon asymmetry. The asymmetry therefore, at least at this energy, is not particularly sensitive to the different choices of the final state interactions of η mesons.

We have also calculated the observables of the reaction using several different proton optical potentials. We found that the calculated observables are rather insensitive to the
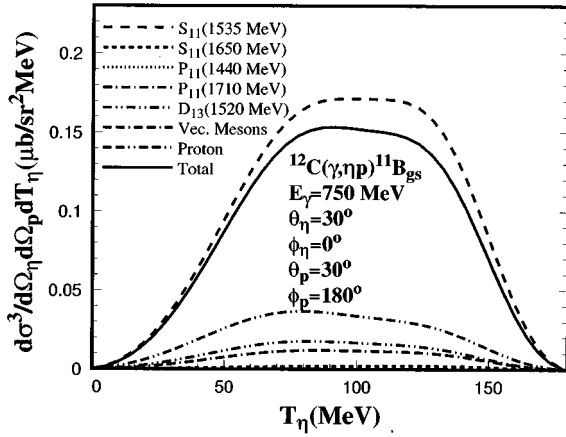
FIG. 5. Contributions of different diagrams to the cross section of the $^{12}C(\gamma, \eta p)^{11}B_{g.s.}$ reaction at photon energies of 750 MeV.

variations among these optical potentials.

The sensitivity of the results to the bound state potentials was also assessed by performing calculations in which different binding potentials are used. In this case relativistic scalar and vector potentials of Woods-Saxon shape [23] were used to generate the Dirac bound state wave function. The results are shown by the dashed curve in Fig. 9(a) along with the results obtained using the Hartree potentials adopted throughout the present study (solid curve). Comparison of these curves indicates the level of sensitivity in our model calculations to the bound state potentials. This comparison shows that the Hartree bound state potentials lead to somewhat larger cross sections at this photon energy. On the other hand, the photon asymmetry calculations appear to be insensitive to different choices of the bound state potentials [Fig. 9(b)].

In addition to the kinematics used above, we also calculated the observables of the reaction for another set of angles for the outgoing particles. The motivation for choosing this new set is to compare the results of our model with those of the nonrelativistic model of Lee *et al.* [8]. Figure 10 shows
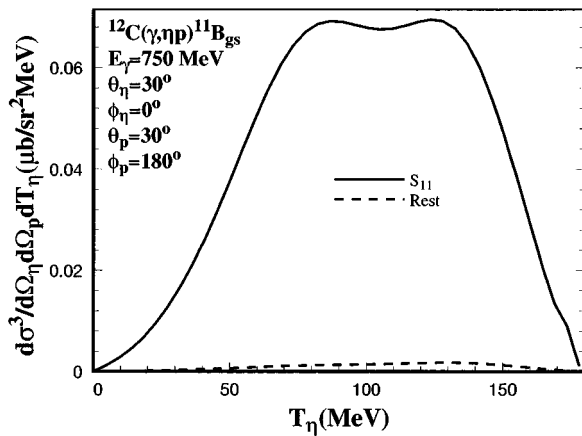

FIG. 6. Differential cross section for the same reaction as Fig. 5, calculated in the distorted wave approximation. Solid curve: DW calculations using only $S_{11}(1535)$ diagrams (curve labeled S_{11}). Long dashed curve: DW calculations using all the diagrams but those of $S_{11}(1535)$ resonance (curve labeled "Rest").
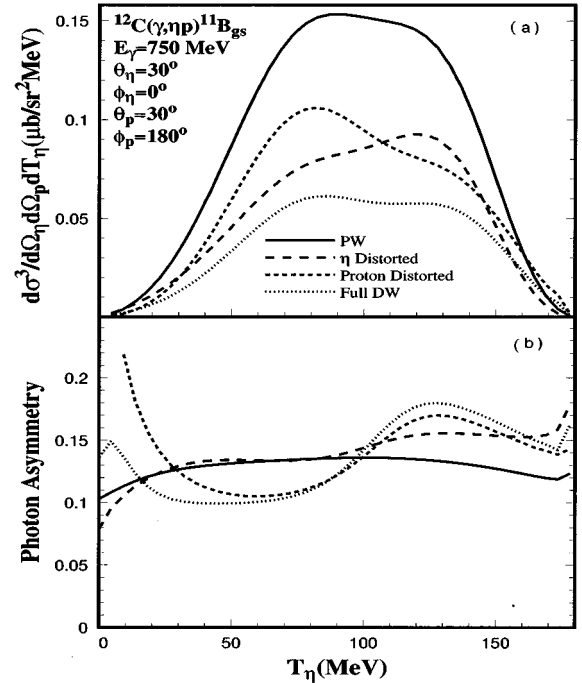

FIG. 7. Differential cross section (a) and photon asymmetry (b) for the reaction $^{12}C(\gamma, \eta p)^{11}B_{g.s.}$ at $E_\gamma = 750$ MeV. The Hartree potentials of Ref. [18] are used in calculation of the bound state wave function. The final state energy-dependent global optical potentials are taken from Ref. [19]. The η optical potential is the DW1 potential of Lee *et al.* [8]. Solid curve: plane wave calculations. Long dashed curve: calculations include only final state interactions of the η meson (η distorted). Short dashed curve: calculations include only final state interactions of outgoing proton (proton distorted). Dotted curve: both η and proton waves are distorted (full DW).

this comparison. The calculations are performed at the following angular settings for the outgoing particles: $\theta_\eta = 20°$, $\phi_\eta = 0°$ and $\theta_p = 15°$, $\phi_p = 180°$. We have plotted the results of the nonrelativistic plane wave calculations of Lee *et al.* [8] together with our results for both plane wave and distorted wave calculations. Figure 10(a) shows the cross section and Fig. 10(b) the resulting photon asymmetry. Results of the relativistic plane wave and distorted wave calculations are shown by solid and short dashed curves, respectively. The nonrelativistic plane wave calculations are depicted by the long dashed curves.

Comparison of the solid and long dashed curves indicates that both relativistic and nonrelativistic calculations produce curves with similar shape, but the nonrelativistic calculations predict generally larger cross sections in the η energy range up to ~ 120 MeV, and fall below at higher η energies. There is also a slight shift in the relative positions of the peaks in the two calculations. As noted earlier, the inclusion of final state interactions leads to a suppression of the calculated cross sections.

The plane wave relativistic and nonrelativistic predictions for the photon asymmetry differ significantly (note that Lee *et al.* use a definition of asymmetry which is opposite in sign to the one used here; for the purpose of the present comparison the results from Ref. [8] have been multiplied by -1). The relativistic calculations produce a flat curve with small
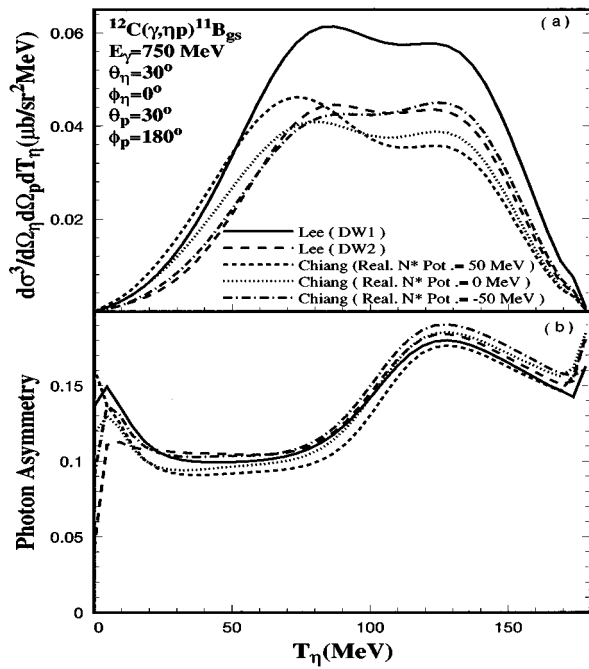
FIG. 8. Same as Fig. 7 but for different choices of η optical potentials. Solid curve: DW calculations using DW1 of Ref. [8]. Long dashed curve: DW calculations using DW2 of Ref. [8]. DW calculations using the optical potential of Ref. [22] with the real part of the S_{11} self-energy set to 50 MeV (short dashed curve), 0 MeV (dotted curve), and -50 MeV (dash-dotted curve).
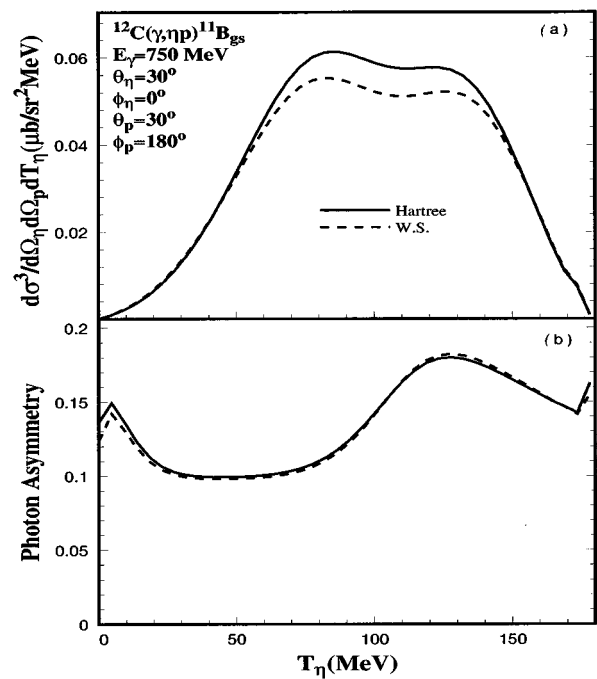

FIG. 9. Differential cross section (a) and photon asymmetry (b) for the same reaction as in Fig. 7. The final state optical potentials for the η meson and outgoing proton are the same as those of Fig. 7. Curves are labeled for different choices of proton bound potentials: Solid curve: DW calculations using Hartree potential of Ref. [18]. Dashed curve: DW calculations using Woods-Saxon potential of Ref. [23].

positive values, whereas the nonrelativistic calculations result in a curve with large negative values, with strong dependence on the η energy. The relativistic calculations show some sensitivity to final state interactions whereas Lee *et al.* report such effects are negligible in the nonrelativistic calculations.

We carried out similar calculations for the photoproduction reaction on a ^{16}O target leading to the ground state in ^{15}N. Figure 11 shows the results of these calculations. The residual nuclear state is assumed to be a pure $1p_{1/2}$ hole state. The Hartree potentials of Ref. [18] are used to calculate the bound state wave function. The final state interactions of the outgoing proton and η meson are calculated using the energy-dependent global optical potential of Ref. [19] and the DW1 optical potential of Ref. [8], respectively.

The results for the cross section are very much similar to the ^{12}C case (see Fig. 7). In the case of ^{16}O we note that the distorted wave cross section (dotted curve) is slightly smaller in comparison with the corresponding case in ^{12}C (dotted curve in Fig. 7). On the other hand, the resulting photon asymmetries for this target behave differently form those of the ^{12}C target. The distorted wave calculations here peak at lower η energies. Moreover, asymmetries for this target have larger magnitudes but this occurs in a region of very small cross sections. These differences with the ^{12}C case indicate that the asymmetry is dependent on the single-particle state from which the proton is ejected.

We have also used our relativistic model for calculations of the reaction on ^{40}Ca. Figure 12 shows the results of our calculations for the case in which the residual nucleus (^{39}K) is left in its ground state (a $1d_{3/2}$ hole state) and the incident

photon energy is 750 MeV. The calculated cross sections of Fig. 12(a) show curves with different shapes from those of the two targets studied previously. The final state interactions of the outgoing particles lead to a suppression of the cross section for this target in a manner similar to what has been noted earlier for ^{12}C and ^{16}O. We find that the earlier observation on photon asymmetries is confirmed in the present case; the photon asymmetry calculations are sensitive to the final state interactions of the outgoing particles. This is in contrast to the predictions of the nonrelativistic model for the reaction [8]. The shape and magnitude of the asymmetries are different from those found for the ^{12}C and ^{16}O targets.

We have also carried out calculations for the observables of the reaction on a ^{40}Ca target leading to an odd parity $1p_{3/2}$ hole state in ^{39}K. The results are shown in Fig. 13. The curves in this figure have the same features as in Fig. 10, except that the differences in the magnitude of the relativistic and nonrelativistic cross sections are larger. Also the effects of the final state interactions are more prominent for the present case. Note that the photon asymmetries given in Figs. 10(b) and 13(b) have approximately the same shapes. These similarities, and the fact that reaction is taking place on a proton in a $1p_{3/2}$ state, support our earlier statement on the state dependence of the asymmetry.

The calculations reported in this section have all used a specific set of coupling constants; one of several that are given in Ref. [4]. The question then arises concerning the sensitivity of the calculated results to the possible differences among these sets which provide nearly equivalent fits to the data for the elementary reactions. We have carried out cal-
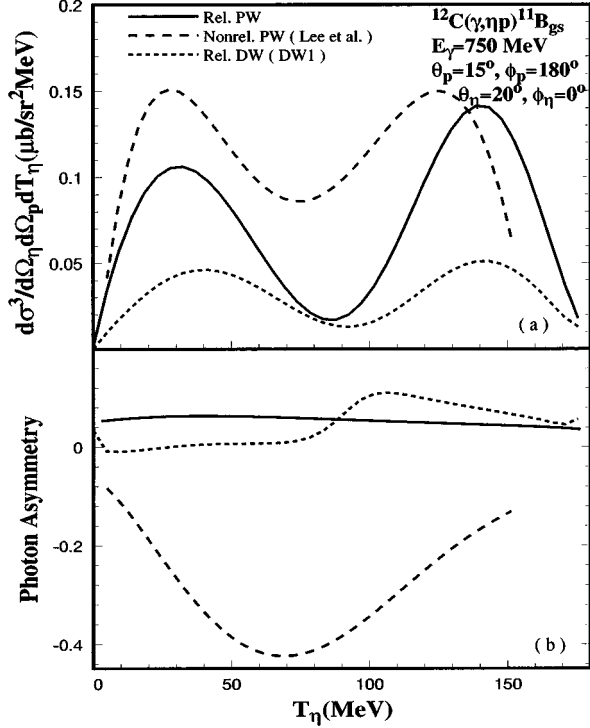
FIG. 10. Differential cross section (a) and photon asymmetry (b) for the same reaction as Fig. 7. Solid curve: relativistic PW calculations. Long dashed curve: nonrelativistic PW calculations of Lee *et al.* [8]. Short dashed curve: relativistic DW calculations.

culations using the set given in the first column of Table V of Ref. [4]. The results show that there are some changes in the magnitudes of the calculated cross sections and photon asymmetries. These changes are at the level of 15% for the cross sections but are somewhat larger for the asymmetries.

IV. CONCLUSIONS

In this paper we have developed a relativistic model for the quasifree photoproduction of η mesons on complex nuclei. The ingredients of the model are that (i) the nucleon wave functions are solutions of the Dirac equation with appropriate scalar and vector potentials consistent with the relativistic mean field approach, (ii) the η meson is described by solutions of the Klein-Gordon equation with appropriate optical potentials, and (iii) the interactions between the fields are introduced through a covariant effective Lagrangian. Contributions from nucleon resonances and t-channel vector mesons as well as the nucleon Born diagrams are included. The model is used to calculate the cross section and photon asymmetry, for different target nuclei. Both plane wave and distorted wave calculations are presented.

We wish to comment on the question of the gauge invariance of the reaction amplitude calculated in the above manner. The effective Lagrangian we start with is gauge invariant. As we look at the nuclear amplitude itself, as given by Eq. (2.19), we find that its invariance is determined by the behavior of the Γ operators given in Eqs. (2.20)–(2.26). All these operators are gauge invariant, except for the electric parts of Eq. (2.20). These latter terms are invariant only in the limit where the particles involved in the elementary in-
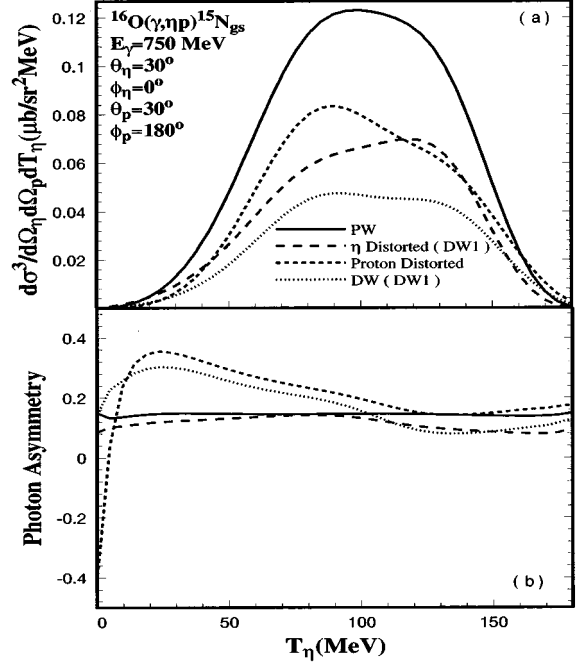

FIG. 11. Differential cross section (a) and photon asymmetry (b) for the reaction $^{16}O(\gamma, \eta p)^{15}N_{g.s.}$ at $E_\gamma = 750$ MeV. The Hartree potential of Ref. [18] is used in calculation of the bound state wave function. The final state energy-dependent global optical potentials are taken from Ref. [19]. The η optical potential is the DW1 potential of Lee *et al.* [8]. Solid curve: plane wave calculations. Long dashed curve: calculations include only final state interactions of the η meson with nuclei (η distorted). Short dashed curve: calculations include only final state interactions of outgoing proton (proton distorted). Dotted curve: both η and proton waves are distorted (DW).

teraction are considered to be on their mass shell.

The energy region where the $S_{11}(1535)$ resonance dominates the reaction is identified. As expected this region is close to threshold and covers a range of photon energies from 750 MeV to 950 MeV. None of the other diagrams makes contributions at the same level as the S_{11}. We find that the next leading diagrams are proton, D_{13} resonance, and vector meson poles. However, we also find that there is some cancellation among these contributions. In our view the energy region identified above is perhaps the best suited for using the η photoproduction reactions to study the properties of the S_{11} resonance in the nuclear medium.

When the final state interactions of the outgoing particles are included, we find that the resulting cross sections are strongly suppressed. The extent of this suppression depends somewhat on the type of optical potential used to represent the final state interaction. We find some variations among the available sets of potentials particularly those that describe the η meson final state interactions. Several η optical potentials were tested and lead to different results for the cross section as well as the photon asymmetry . The uncertainty in η optical potentials makes it difficult to make final predictions for the cross sections. More theoretical work on the final state interactions of the η is required.

Calculations were carried out using the same kinematics as those in the recent nonrelativistic calculations of Lee *et al.* [8]. Results of our calculations for the cross section have
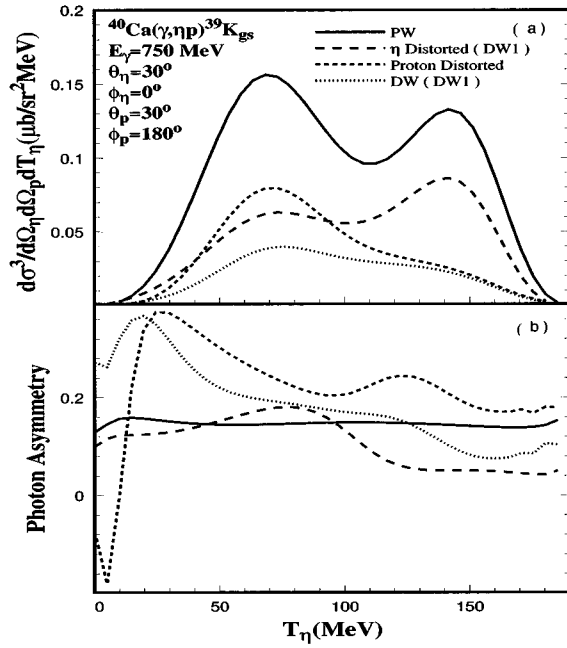
FIG. 12. Differential cross section (a) and photon asymmetry (b) for the reaction ^{40}Ca$(\gamma, \eta p)^{39}$K$_{g.s.}$ at $E_\gamma = 750$ MeV. The Hartree potential of Ref. [18] is used in the calculation of the bound state wave function. The final state energy-dependent global optical potentials are taken from Ref. [19]. The η optical potential is the DW1 potential of Lee *et al.* [8]. Solid curve: plane wave calculations. Long dashed curve: calculations include only final state interactions of the η meson with nuclei (η distorted). Short dashed curve: calculations include only final state interactions of outgoing proton (proton distorted). Dotted curve: both η and proton waves are distorted (DW).

shapes close to those of these nonrelativistic calculations but the magnitudes of our results are somewhat smaller. In contrast, the photon asymmetries predicted by the two models differ significantly. The nonrelativistic model gives large asymmetries in the plane wave limit, which are found to be insensitive to the final state interactions of the outgoing particles. Our predictions yield much smaller asymmetries and these are strongly affected by the final state interactions. Lee *et al.* have also found that a small percentage change in the masses of the S_{11} and D_{13} have large effects on the cross sections and the asymmetries, respectively. Our present calculations show similar effects. These are indications that eta photoproduction reactions can be used as a probe of medium modifications of the properties of these resonances. These of course are expected to go beyond the simple mass shifts; for example, there may in fact be a radial density dependence of the masses of the propagators. Studies of these effects with the present relativistic model are planned.

The above statements indicate that the present reaction is rich in its physics content. If enough data become available, one will be able to clarify the role played by the intermediate
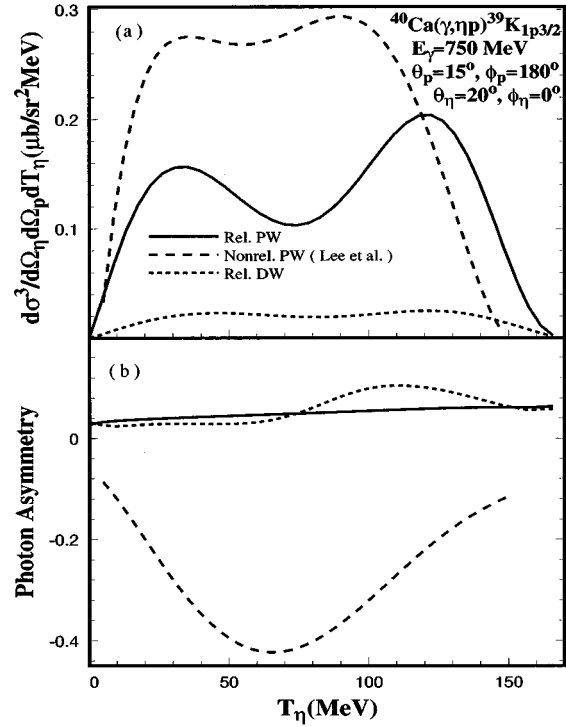

FIG. 13. Differential cross section (a) and photon asymmetry (b) for the same reaction as Fig. 12. The reaction is assumed to take place in $1p_{3/2}$ proton. The potentials are the same as those of Fig. 12. Curves are labeled as in Fig. 10.

nucleon states (the S_{11} and the D_{13}) as well as the vector mesons while embedded in the nuclear environment. The question of the optical potential for the η-nucleus system could also be clarified. The data could also be used to assess the need for a strictly relativistic treatment. It is clear that there is a multiplicity of effects at play and hence it is imperative that measurements at several energies in the region discussed above and for a variety of target nuclei be carried out. Measurements of the cross sections and photon asymmetries in exclusive production, as well as coherent production, will be very helpful in shedding more light on the above issues. In a subsequent paper the present model will be extended to the treatment of inclusive reactions for which some data have become available recently [3].

ACKNOWLEDGMENTS

[1] F. Plouin *et al.*, Phys. Lett. B **276**, 526 (1992).

[2] R. S. Kessler *et al.*, Phys. Rev. Lett. **70**, 892 (1993).

[3] M. Roebig-Landau *et al.*, Phys. Lett. B **373**, 45 (1996); M. Vineyard (private communication).

[4] M. Benmerrouche, Nimai C. Mukhopadhyay, and J. F. Zhang, Phys. Rev. D **51**, 3237 (1995).

[5] C. Bennhold and H. Tanabe, Phys. Lett. B **243**, 13 (1990).

[6] C. Bennhold and H. Tanabe, Nucl. Phys. **A530**, 625 (1991).

[7] L. Tiator, C. Bennhold, and S. S. Kamalov, Nucl. Phys. **A580**, 455 (1994).

[8] F. X. Lee, L. E. Wright, C. Bennhold, and L. Tiator, Nucl. Phys. **A603**, 345 (1996).

[9] M. Hedayati-Poor, J. I. Johansson, and H. S. Sherif, Nucl. Phys. **A539**, 337 (1995).

[10] M. Hedayati-Poor, J. I. Johansson, and H. S. Sherif, Phys. Rev. C **51**, 2044 (1995).

[11] J. D. Walecka, Ann. Phys. (N.Y.) **83**, 491 (1974).

[12] B. D. Serot and J. D. Walecka, in *Advances in Nuclear Physics*, edited by J. W. Negele and E. Vogt (Plenum, New York, 1986), Vol. 16.

[13] C. Bennhold and L. E. Wright, Phys. Lett. B **191**, 11 (1987).

[14] M. Hedayati-Poor and H.S. Sherif, in *Proceedings of the XIV International Conference on Particles and Nuclei,* Williamberg, 1996, edited by C. Carlson and J. Domingo (World Scientific, Singapore, 1997).

[15] F. Mandl and G. Shaw, *Quantum Field Theory* (Wiley, New York, 1984).

[16] J. I. Johansson and H. S. Sherif, Nucl. Phys. **A575**, 477 (1994).

[17] S. Frullani and J. Mougey, in *Advances in Nuclear Physics*, edited by J.W. Negele and E. Vogt (Plenum, New York, 1984), Vol. 14, p. 1.

[18] C. J. Horowitz and B. D. Serot, Nucl. Phys. **A368**, 503 (1986).

[19] E. D. Cooper, S. Hama, B. C. Clark, and R. L. Mercer, Phys. Rev. C **47**, 297 (1993).

[20] M. Batinić, I. Šlaus, A. Švarc, and B. M. K. Nefkens, Phys. Rev. C **51**, 2310 (1995).

[21] M. Batinić, I. Dadić, I. Šlaus, and A. Švarc, e-print nucl-th/9703023.

[22] H. C. Chiang, E. Oset, and L. C. Liu, Phys. Rev. C **44**, 734 (1991).

[23] G. Lotz, Ph.D. thesis, University of Alberta, 1989.